CCS Chemistry

COMMUNICATION

Received: Mar. 16, 2022 | Accepted: Apr. 6, 2022 | Published: May 10, 2022

Generation of Hierarchical Pores in Metal–Organic Frameworks by Introducing Rigid Modulator

Zhiwen Ai, Long Jiao, Jingxue Wang & Hai-Long Jiang*

Department of Chemistry, University of Science and Technology of China, Hefei, Anhui 230026

**Corresponding author: jianglab@ustc.edu.cn*

Cite this: *CCS Chem*. **2022**, 4, 3705–3714
DOI: 10.31635/ccschem.022.202201974

The fabrication of hierarchically porous metal–organic frameworks (HP-MOFs) that combine tunable mesopore sizes with high stability is highly desired but remains a technical challenge. Herein, a facile and versatile "rigid modular-assisted defect formation" strategy has been developed to transform microporous MOFs into their corresponding HP-MOFs. By controlling the modulator dose and acid amount, the pore size and mesopore percentage can be finely regulated. Based on the hierarchical pores, the mass transfer of molecules with large sizes is significantly promoted. As a result, the representative HP-UiO-66-NH_2-OTf, decorated with a trifluoromethanesulfonate (OTf) group to enhance Lewis acidity, exhibits excellent activity and selectivity in tandem catalysis, far superior to pristine UiO-66-NH_2. This work provides a novel strategy to the general synthesis of stable HP-MOFs.

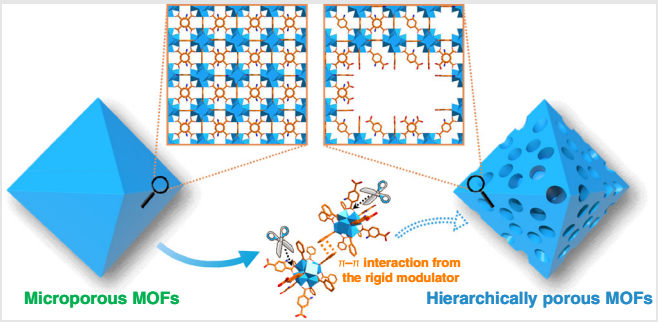

Keywords: **hierarchically porous materials, metal–organic frameworks, rigid modulators, heterogeneous catalysis, stability**

Introduction

Metal–organic frameworks (MOFs), a class of porous crystalline materials constructed by metal nodes and organic linkers, have attracted significant research interests in the last two decades.[1–3] The well-defined crystalline structure, highly tunable pore geometry, diverse components, and large surface area of MOFs make them very promising in gas adsorption/separation, catalysis, and many other applications.[4–6] Traditionally, most MOFs typically present intrinsic microporous characteristics, endowing them with unique features for small-molecule access, realizing molecular sieving and size-selective catalysis.[7–9] Unfortunately, microporous MOFs are unfavorable for large molecule diffusion, thereby hampering applications involving large-size molecules.[10–14] In view of this, the fabrication of stable MOFs with controlled mesopores/macropores is highly desired.

One straightforward method for pore size enlargement is to elongate the length of bridging linkers to fabricate mesoporous MOFs.[15–17] However, when the linker becomes longer, the fabrication of the targeted MOFs becomes more challenging due to the complicated synthesis of the linker precursor.[18,19] Meanwhile, the stability of resulting MOFs with long linkers is usually unsatisfactory,[15,20] and framework interpenetration inevitably minimizes the energy of the system.[21–23] The generation of additional mesopores/macropores in stable microporous MOFs has been recognized to be an alternative promising way.[24–26] The inherent micropores of hierarchically

DOI: 10.31635/ccschem.022.202201974
Citation: *CCS Chem*. **2022**, 4, 3705–3714
Link to VoR: https://doi.org/10.31635/ccschem.022.202201974

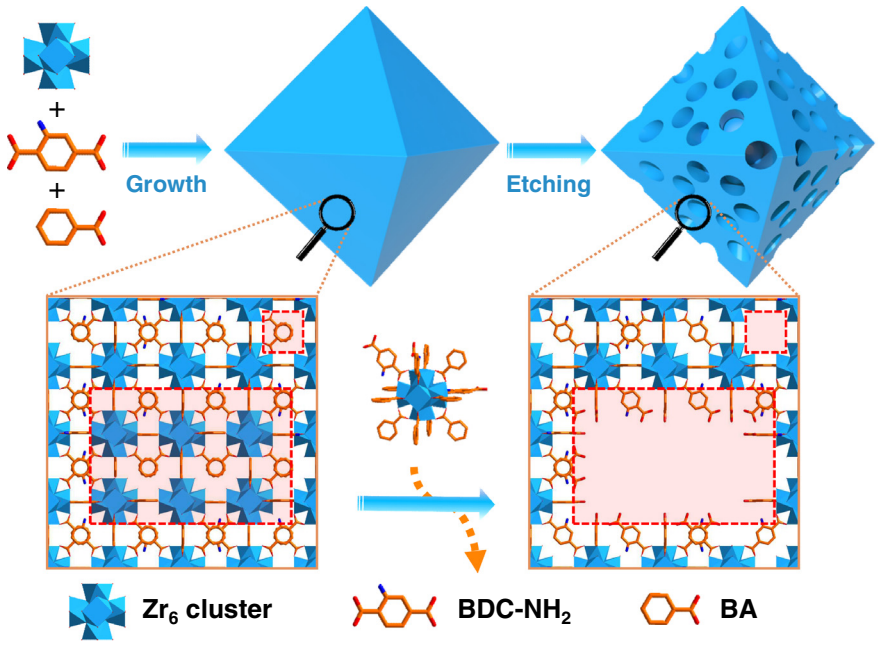

Scheme 1 | *Schematic illustration showing the synthesis of HP-MOFs with BA as the modulator, by taking HP-UiO-66-NH_2 as a representative material.*

porous MOFs (HP-MOFs) provide high surface area and ample active sites, and the mesopores/macropores facilitate the transport of large molecules, greatly extending the application fields of MOFs.[27]

Along with the second line, different strategies have been developed to afford HP-MOFs, including soft/hard template, template-free, ligand fragment or thermal fracture, laser photolysis, and so on.[27–34] Most of these reported methods have specific requirements, making the synthesis of HP-MOFs hard to control and/or only suitable for particular MOF systems. Recently, the defect-formation method, generating a large number of defects using alkyl monocarboxylic acid as a modulator to produce mesopores, seems convenient and extendable to other MOF systems.[35–37] In spite of the great promise, the introduced mesopore sizes of the modulators are restricted via steric effects, in which the length of the alkyl modulators should be carefully chosen as a very long modulator gives too weak coordination ability while a short one cannot create suitable steric effects. Therefore, it is of great interest to create the large steric effect by small modulators in a simple way to generate large mesopore sizes.

Herein, by introducing a large number of small yet rigid modulators with significant steric effects during the synthesis of MOFs, the defects can be easily created and gathered in the MOF skeleton (Scheme 1). Upon acid etching, the defective metal clusters with a few remaining bonds are not very stable and can be removed, leaving mesopores with varied sizes in the MOFs. In contrast, the metal clusters without defects can be well retained to maintain the pristine MOF skeleton and stability. As a result, HP-MOFs integrating the stability of the pristine microporous MOFs with additional hierarchical pores can be obtained. Moreover, the size and content of the mesopores can be readily regulated by changing modulator concentration and/or acid etching conditions. Such a synthetic strategy has been successfully extended to different structural types of MOFs. Taking HP-UiO-66-NH_2 as a representative material, it is rich in Brønsted acid sites due to the exposed free carboxylic acid of linkers resulting from the removal of Zr-oxo clusters, and large functional species can be encapsulated inside the mesopores (Scheme 1). By further modifying the Zr-oxo clusters with a trifluoromethanesulfonate (OTf) group, the obtained HP-UiO-66-NH_2-OTf exhibits excellent catalytic activity and selectivity in the tandem multicomponent deacetalization-acetalization reaction, providing synergistic advantages of abundant micropores and defective mesopores.

Results and Discussion

The microporous MOF, UiO-66-NH_2 (formulated $Zr_6O_4(OH)_4(BDC\text{-}NH_2)_6$, BDC-$NH_2$=2-amino-1,4-benzenedicarboxylate) was selected as a representative material, which is a widely used MOF with high chemical/thermal stability and diverse functional properties. Typically, benzoic acid (BA), which is intensively adopted as the modulating agent in Zr-MOF synthesis, is investigated. By gradually increasing the amount of BA, a series of UiO-66-NH_2/BA_x (x represents the BA amount

DOI: 10.31635/ccschem.022.202201974
Citation: *CCS Chem.* **2022**, 4, 3705–3714
Link to VoR: https://doi.org/10.31635/ccschem.022.202201974

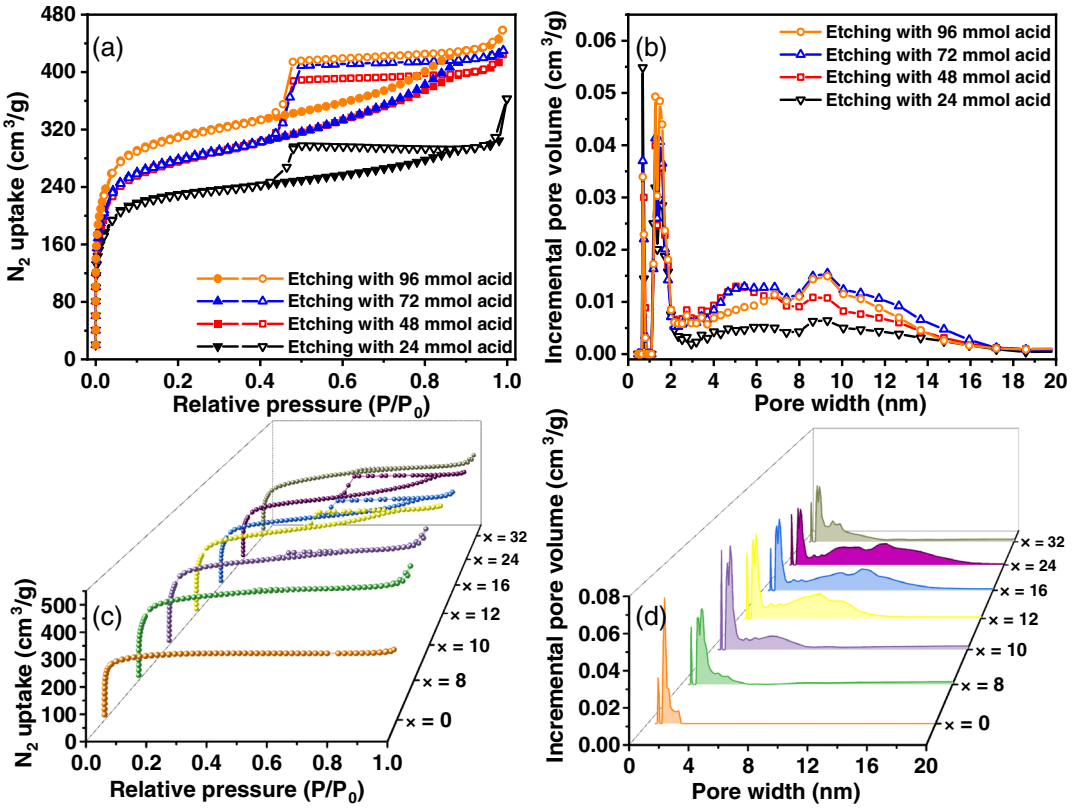

Figure 1 | *(a) N_2 sorption isotherms at 77 K and (b) the corresponding pore size distributions based on the density functional theory (DFT) model for UiO-66-NH_2/BA_{24} after etching with varying amounts of formic acid. (c) N_2 sorption isotherms at 77 K and (d) the corresponding pore size distributions based on the DFT model for HP-UiO-66-NH_2/BA_x synthesized with varying amounts of BA and subsequently etching with 72 mmol formic acid (x represents the amount of BA introduced in the synthesis, x = 0, 8, 10, 12, 16, 24, and 32 mmol).*

introduced in the synthesis, x = 0, 8, 10, 12, 16, 24, and 32 mmol) has been constructed (see Supporting Information Figure S1a). Obviously, mesopores cannot be generated with the introduction of only the modulator (see Supporting Information Figure S2). In using UiO-66-NH_2/BA_{24} as a representative material, different amounts of formic acid are adopted in the etching process to generate potential mesopores (see Supporting Information Figure S1b). With the increased content of formic acid, the surface area and mesopore volume increase to varying degrees, whereas the mesopore size range is almost maintained (Figures 1a and 1b). Once the acid amount exceeds 72 mmol, the mesopore no longer increases. The ^{1}H NMR spectra show that BA is completely removed to liberate the mesopores after etching with 24 mmol formic acid (see Supporting Information Figures S3a and S3b). Meanwhile, Zr species can be clearly detected in the supernatant by inductively coupled plasma atomic emission spectrometry after the acid etching process (see Supporting Information Table S1), showing that the Zr clusters are etched away during mesopore formation. However, to release mesopores as much as possible by etching out the unstable dangling Zr-oxo clusters, the optimized amount of formic acid was found to be 72 mmol, at which the largest pore volume is obtained (Figure 1b).

Given that the largest pore volume is generated with 72 mmol formic acid, all of the microporous UiO-66-NH_2/BA_x are converted to the corresponding HP-UiO-66-NH_2/BA_x with different hierarchical pores by acid treatment with 72 mmol formic acid (see Supporting Information Figure S4). It can be seen that HP-UiO-66-NH_2/BA_0 without the use of BA shows microporosity only (Figures 1c and 1d). Upon the addition of a small amount (8 mmol) of BA, only a small amount of mesopores is produced in HP-UiO-66-NH_2/BA_8, which gives a slight hysteresis loop in the N_2 sorption isotherms (Figure 1c). When the amount of BA is greater than 8 mmol, the mesopores start to be gradually produced. The hysteresis loop becomes apparent when increasing the amount of BA to 10 mmol (Figure 1c). This indicates that a relatively small amount of BA (<8 mmol) can only introduce localized defects, which makes it difficult to create mesopores.[38] Therefore, the corresponding mesopores can be produced when reaching a certain number of BA molecules coordinated to Zr-oxo clusters. As the

DOI: 10.31635/ccschem.022.202201974
Citation: *CCS Chem.* **2022**, 4, 3705–3714
Link to VoR: https://doi.org/10.31635/ccschem.022.202201974

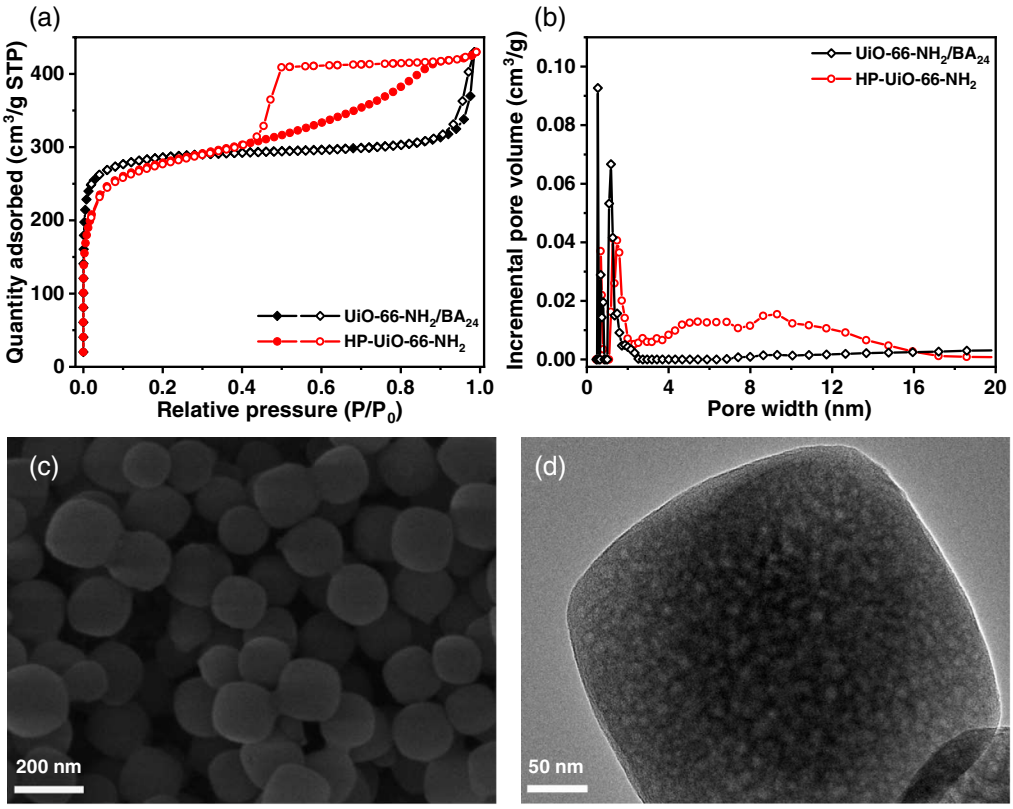

Figure 2 | *(a) N_2 sorption isotherms at 77 K and (b) the corresponding pore size distributions of UiO-66-NH_2/BA_{24} and HP-UiO-66-NH_2 evaluated by the DFT model. (c) SEM and (d) TEM images of HP-UiO-66-NH_2.*

BA amount increases from 10 to 24 mmol, the pore size starts to gradually expand and the mesopore volume becomes prominent in HP-UiO-66-NH_2/BA_x (x = 10~24). When the BA amount reaches 32 mmol, the mesopores vanish unexpectedly, giving rise to the disappearance of the hysteresis loop in N_2 sorption isotherms for HP-UiO-66-NH_2/BA_{32} (Figures 1c and 1d). With severely excessive BA, it is assumed that the defective Zr-oxo clusters are hard to coordinate with the dicarboxylic acid linkers because the BA modulator suppresses the deprotonation of linkers and is replaced by the linkers. From the above results, with 72 mmol formic acid etching, 24 mmol is the optimized BA amount for the creation of the mesoporous structure. The resulting HP-UiO-66-NH_2/BA_{24}, simply denoted as HP-UiO-66-NH_2 for clarity hereafter, presents the largest hysteresis loop with a pore size up to 17 nm (Figure 1d).

Prior to acid etching, N_2 sorption isotherms of UiO-66-NH_2/BA_{24} present a type I curve and suggest a pore size less than 2 nm, clearly illustrating its microporous features (Figures 2a and 2b). Upon formic acid etching for UiO-66-NH_2/BA_{24}, mesopores are generated. The Brunauer–Emmett–Teller (BET) surface area of HP-UiO-66-NH_2 (881 m^2 g^{-1}) is similar to that of the pristine UiO-66-NH_2/BA_{24} (869 m^2 g^{-1}) (Figure 2a). The pronounced hysteresis loop can be observed in the N_2 sorption isotherms of HP-UiO-66-NH_2, obviously demonstrating the mesoporous feature. In sharp contrast with microporous UiO-66-NH_2/BA_{24}, HP-UiO-66-NH_2 suggests a very large mesopore size in the range of 2–17 nm (Figure 2b).[35] Scanning electron microscopy (SEM) imaging shows the retained octahedral morphology of HP-UiO-66-NH_2 (Figure 2c and see Supporting Information Figure S5). Meanwhile, the uniform mesopores are well observed in the transmission electron microscopy (TEM) image of HP-UiO-66-NH_2 in contrast to UiO-66-NH_2 (Figure 2d and see Supporting Information Figure S6), which aligns with the pore size distribution analysis (Figure 2b).

To determine the specific roles of BA, a series of control experiments were performed. First, different flexible alkane monocarboxylic acids (formic acid or acetic acid), with 1 equiv BA, are employed to replace the rigid BA during the synthesis of UiO-66-NH_2 (denoted as UiO-66-NH_2/C_x, x = carbon number). When formic acid is introduced, no hysteresis loop or mesopore is observed in the N_2 sorption isotherms of UiO-66-NH_2/C_1 (see Supporting Information Figure S7). Upon switching formic acid to acetic acid, the widely used modulator in the synthesis of UiO-66-NH_2, no mesopores are generated (see Supporting Information Figure S8). The ^{1}H NMR spectra and thermogravimetric analysis curves reveal

DOI: 10.31635/ccschem.022.202201974
Citation: *CCS Chem.* **2022**, 4, 3705–3714
Link to VoR: https://doi.org/10.31635/ccschem.022.202201974

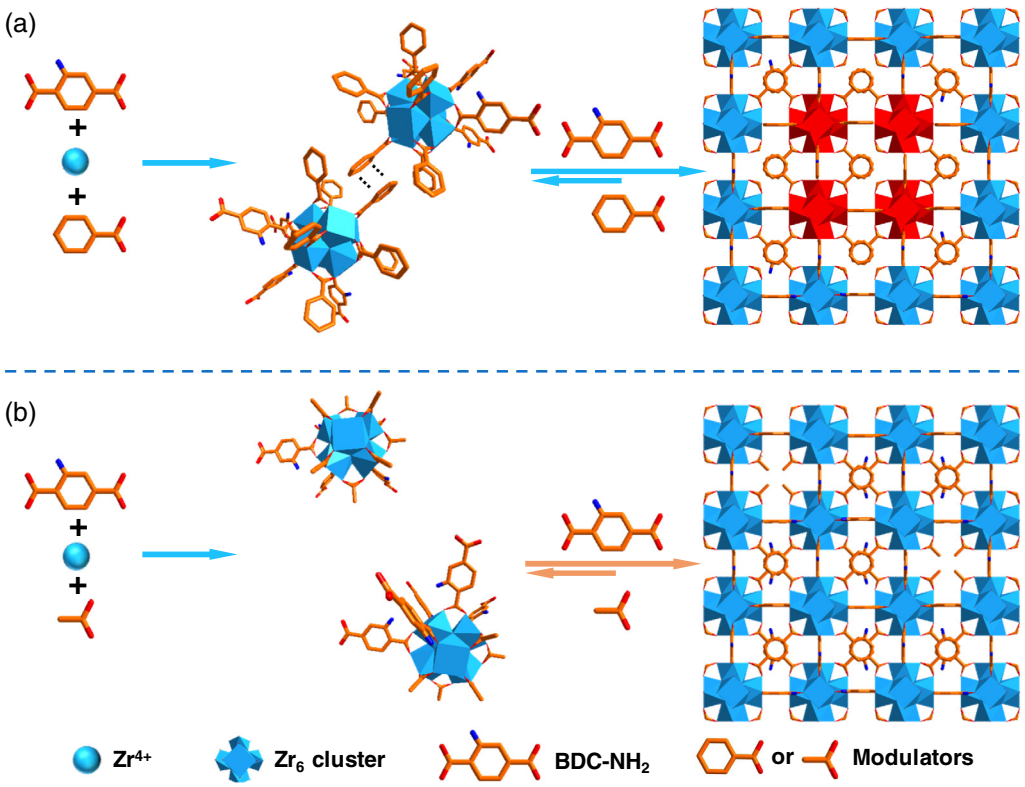

Scheme 2 | *Proposed mechanism for the different roles of (a) rigid modulators and (b) flexible modulators in MOF growth. The Zr-oxo clusters coordinated with too many rigid modulators (BA) as the majority of ligands, highlighted in red, are readily removed by acid etching to generate the mesopore.*

that the average number of acetic acid molecules coordinated to the Zr-oxo cluster is less than that of BA (1.82 vs. 3.26), possibly due to the relatively weaker coordination ability of acetic acid (see Supporting Information Figures S9a and S9d). However, even the corresponding number of acetic acid molecules is close to the number of BA molecules in UiO-66-NH_2/BA_{24}, yet no mesopores can be obtained (see Supporting Information Figures S9e, S9f, and S10). Considering that these two acids are shorter than BA, propionic acid and butyric acid (similar to BA in length) have been further adopted as modulators. However, we still failed to produce mesopores (see Supporting Information Figures S11 and S12). Even a slightly longer ligand, hexanoic acid, was used, but the resulting UiO-66-NH_2/C_6 after acid etching exhibited type I isotherms with pore sizes smaller than 2 nm (see Supporting Information Figure S13). It should be noted that the modulators used above are flexible and have weaker steric effects than the rigid BA, suggesting that the steric effect may be a critical factor in the generation of mesopores.

To further support this assumption, other rigid modulators similar to BA, such as 2-fluorobenzoic acid (2-FBA), were attempted in the synthesis of UiO-66-NH_2. As expected, upon the introduction of 2-FBA, HP-UiO-66-NH_2/2-FBA, with a significant hysteresis loop in the N_2 sorption isotherm, was successfully synthesized and showed size distribution in the mesopore region (see Supporting Information Figure S14). Moreover, 2-naphthoic acid (2-NA), another rigid modulator longer than BA and 2-FBA, was also employed. The resulting HP-UiO-66-NH_2/2-NA, featuring a large hysteresis loop in its N_2 sorption isotherms, presents a wide pore size range of 1–48 nm (see Supporting Information Figure S15). TEM observation clearly observes the large mesopores in HP-UiO-66-NH_2/2-NA (see Supporting Information Figure S15b).

Comparing the different behaviors of flexible and rigid modulators for mesopore generation, it can be inferred that the rigid small-molecule modulators (BA, 2-NA, etc.) generate mesopores from the skeleton with defects, while flexible modulators with alkyl chains cannot. The working principle of MOF growth in the presence of the modulator is illustrated in detail (see Supporting Information Section 5). The Zr-oxo clusters coordinated with too many rigid modulators (such as BA) as the majority of ligands tend to aggregate in a region due to the π–π interactions and steric effects from the benzene ring (Scheme 2a),[39,40] giving rise to the instability of these Zr-oxo clusters because of the lesser coordination with the multi-connected linkers in the "defective region." This region is vulnerable to acid attack, which causes

DOI: 10.31635/ccschem.022.202201974
Citation: *CCS Chem.* **2022**, 4, 3705–3714
Link to VoR: https://doi.org/10.31635/ccschem.022.202201974

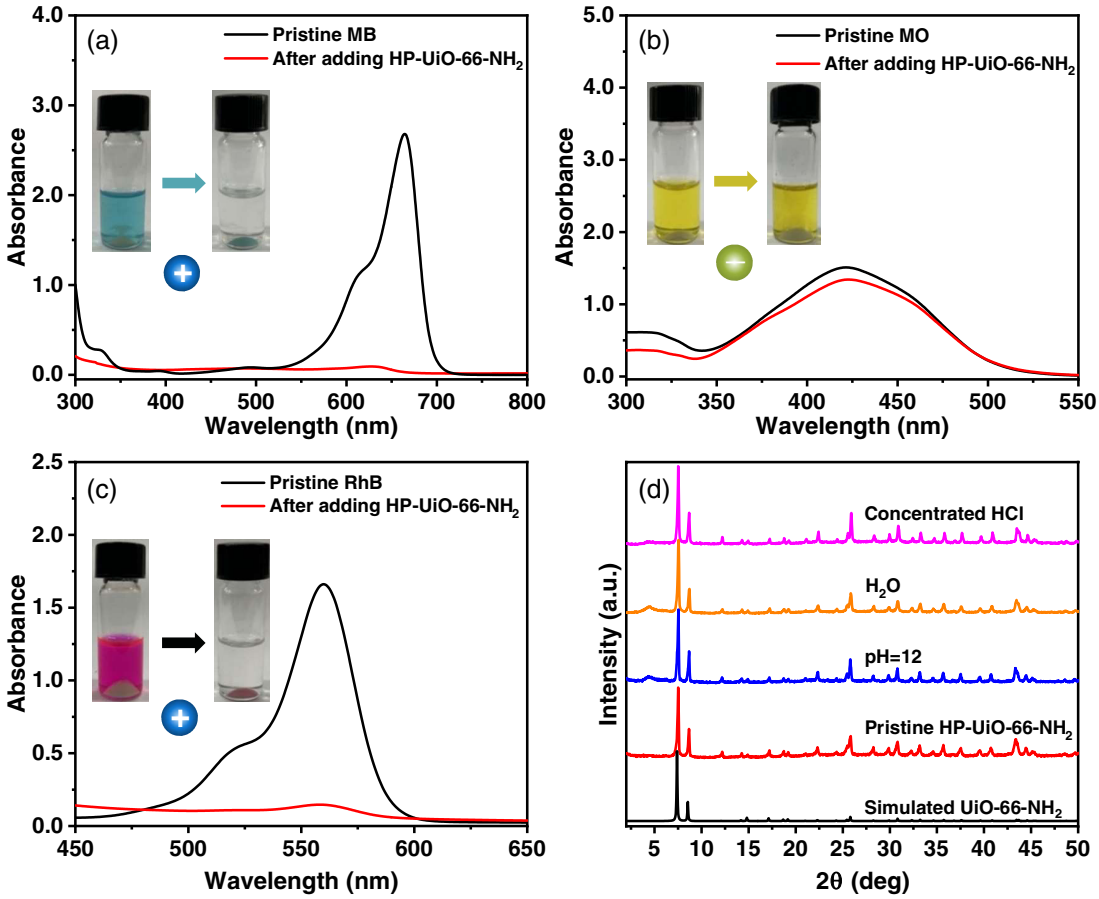

Figure 3 | *UV–vis absorption spectra recording the adsorption of (a) small cationic dye (MB), (b) small anionic dye (MO), and (c) large anionic dye (RhB) after adding HP-UiO-66-NH$_2$. Insets: photos of dye solution (left) before and (right) after adding HP-UiO-66-NH$_2$. (d) PXRD patterns of HP-UiO-66-NH$_2$ after treatment under different conditions for 24 h.*

additional mesopores to be generated by acid etching. Nevertheless, when severely excessive BA (reaching 32 mmol) is used, some of them remain uncoordinated to hamper the interactions between defective Zr-oxo clusters, resulting in a reduced growth rate and an inability to create mesopores (see Supporting Information Section 5). Therefore, larger mesopores would be formed by reasonably increasing the amount and size of the rigid modulators.

In contrast, flexible modulators possess a higher degree of spatial freedom and lack the interactions. The distribution of corresponding defects is uniform in the skeleton, leading to a majority of ligands coordinated to the clusters existing as bridging BDC-NH$_2$ linkers (Scheme 2b). The defective Zr-oxo clusters with bridging linkers as the majority are stable and will not be etched away from the skeleton when attacked by acid. Accordingly, the use of flexible modulators to generate mesopores requires not only the alkyl modulators in a reasonable range of length but also an insufficient amount of bridging linkers.[35]

To provide visible evidence to the naked eye of the generation of mesopores, a series of adsorption experiments on dyes with different kinds of charges have been carried out using HP-UiO-66-NH$_2$. It is shown that a smaller-sized cationic dye, such as methylene blue (MB), is easily absorbed, while a smaller-sized anionic dye, such as methyl orange (MO), is barely captured, further manifesting the anionic MOF skeleton due to the missing Zr-oxo clusters (Figures 3a and 3b). When HP-UiO-66-NH$_2$ is immersed in a dimethylformamide solution of the large cationic dye rhodamine B (RhB), the solution gradually fades and is accompanied by the yellow HP-UiO-66-NH$_2$ turning to bright red (Figure 3c). In contrast, the pristine UiO-66-NH$_2$ neither absorbs the cationic dye RhB nor uptakes anionic dye R250, due to their sizes being larger than the microporous openings (see Supporting Information Figure S16). This direct comparison again manifests the presence of defective mesopores in HP-UiO-66-NH$_2$. Considering the cationic Zr-oxo clusters in UiO-66-NH$_2$, the anionic skeleton should be attributed to the removal of these clusters, leaving behind excessive BDC-NH$_2$ with uncoordinated carboxyl groups. The Fourier transform infrared spectroscopy analysis suggests that an absorption band at 1686 cm^{-1}, which is assigned to free

DOI: 10.31635/ccschem.022.202201974
Citation: *CCS Chem.* **2022**, 4, 3705–3714
Link to VoR: https://doi.org/10.31635/ccschem.022.202201974

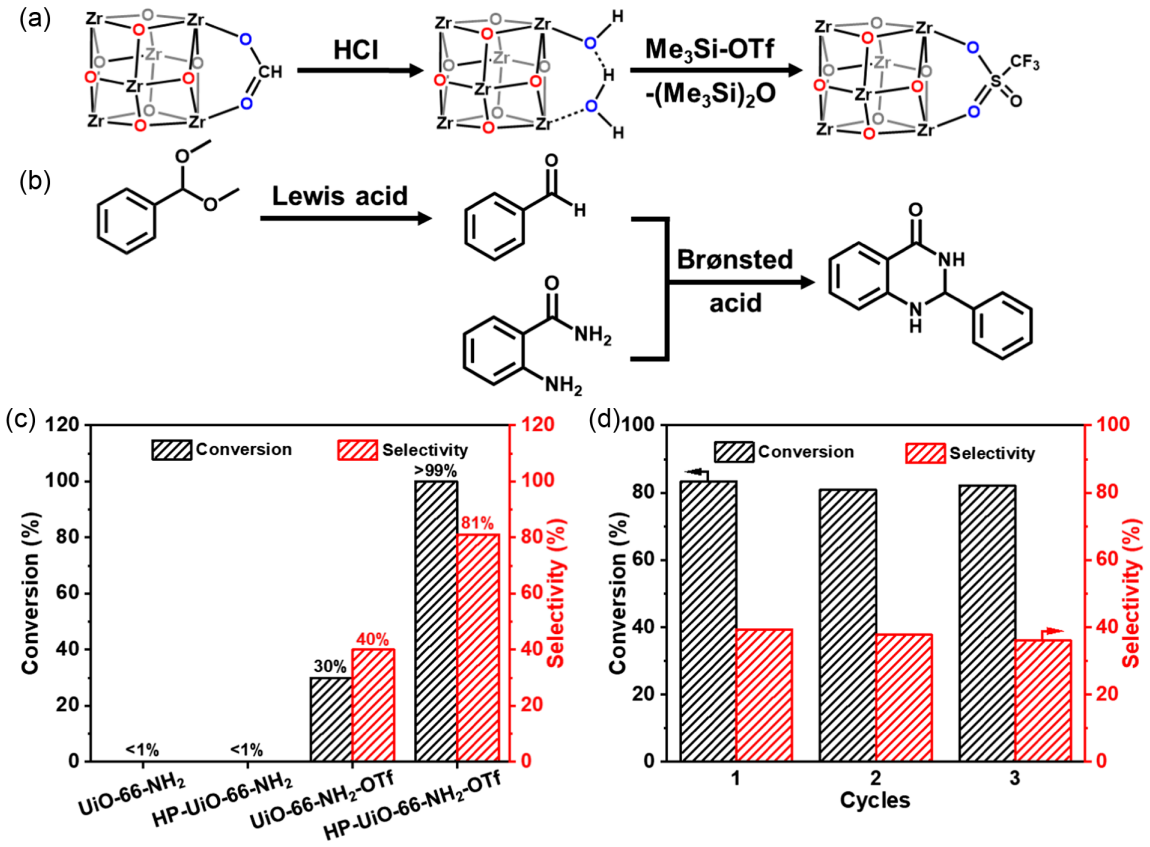

Figure 4 | *(a) Post-synthetic activation of HP-UiO-66-NH_2 by acid treatment followed by triflation to HP-UiO-66-NH_2-OTf with Lewis acidity. (b) Illustration of the Lewis-Brønsted acid tandem catalysis for the synthesis of 2,3-dihydroquinazolin-4(1H)-one. (c) Conversion of tandem deacetalization-acetalization catalysis over UiO-66-NH_2, HP-UiO-66-NH_2, UiO-66-NH_2-OTf, and HP-UiO-66-NH_2-OTf. (d) Recycling test of the tandem catalysis with epibromohydrin over HP-UiO-66-NH_2-OTf.*

carboxylic acid in BDC-NH_2, is observed for HP-UiO-66-NH_2 while it is absent in the pristine microporous MOF (see Supporting Information Figure S17).[41,42] This confirms that the origin of the anionic framework comes from the uncoordinated carboxyl group of the BDC-NH_2 linkers in the skeleton due to the missing of Zr-oxo clusters. In the supernatant of the acid etching process, BA is detected while the BDC-NH_2 linker is not shed from the skeleton (see Supporting Information Figure S18), indicating that bridging linkers remained in the mesoporous framework. These results indicate that HP-UiO-66-NH_2 features an anionic mesoporous framework and involves Zr-oxo cluster defects and free carboxyl groups dangling onto the skeleton.

Based on the above results, the mechanism of the rigid modulator-induced Zr-oxo cluster missing can be summarized. By using a small amount of the rigid modulator (e.g., BA) coordinating to the Zr-oxo clusters, these clusters coordinated with the bridging linker (BDC-NH_2) as the majority are stable and will not be etched from the framework. As the BA amount increases, the multi-defective region is generated where BA accumulates. Some of the Zr-oxo clusters coordinating with too many BA rather than BDC-NH_2 become progressively unstable and are easily etched by acid attack to produce mesopores (Scheme 1). The missing Zr-oxo clusters leave behind the uncoordinated carboxyl group of dicarboxylic acids, accordingly creating an anionic skeleton.[43] When the BA continues to increase, more unstable clusters are produced, leading to more prominent mesopores.

It is worth noting that the generation of mesopores in HP-UiO-66-NH_2 does not significantly affect its inherent micropores. Moreover, the stability investigation shows that HP-UiO-66-NH_2 shows good chemical stability in solutions ranging from concentrated HCl to alkaline solutions (pH 12), similar to the pristine UiO-66-NH_2 (Figure 3d and see Supporting Information Figure S19). These results suggest that HP-MOFs synthesized by this method can simultaneously own hierarchical pores and high stability.

To illustrate the generality of this synthetic strategy, UiO-66 with different functional groups, such as HP-UiO-66 and HP-UiO-66-NO_2, have been successfully synthesized with hysteresis loops in N_2 sorption curves and their

DOI: 10.31635/ccschem.022.202201974
Citation: *CCS Chem.* **2022**, 4, 3705–3714
Link to VoR: https://doi.org/10.31635/ccschem.022.202201974

corresponding pore sizes extend to 16 and 12 nm, respectively (see Supporting Information Figures S20 and S21). Furthermore, different types of stable MOFs, such as MIL-53 and DUT-5, have also been examined by adopting this rigid modulator approach. As expected, the corresponding hierarchically porous structures can be prepared and inherit the remarkable chemical stability of their parent MOFs (see Supporting Information Figures S22–S25), unambiguously supporting the generality of this synthetic strategy.

Based on the obtained hierarchically porous structures, the mesopores of HP-MOFs facilitate rapid substrate transport and enhance mass transfer in comparison to their microporous counterparts. Moreover, the defective sites in HP-MOFs can act as catalytic centers and/or be easily modified, further improving catalytic performance. As a proof of concept, HP-UiO-66-NH_2-OTf was synthesized by introducing the OTf group on the exposed Zr-oxo clusters through an acid reaction as a prerequisite (Figure 4a and see Supporting Information Figure S26).[42,44] Although the –NH_2 group on the BDC-NH_2 linker is detrimental to the MOF acidity, the introduction of such an OTf group would provide strong Lewis acidity of the Zr-oxo clusters.[45] In the diffuse reflectance infrared Fourier transform spectra of HP-UiO-66-NH_2-OTf, the reduced peaks of the terminal –OH/–OH_2 and μ_3-OH at 3672 and 2745 cm^{-1} support that the OTf groups are anchored onto the Zr-oxo clusters (see Supporting Information Figures S27 and S28).

The HP-UiO-66-NH_2-OTf has been employed for the tandem catalysis of 2-aminobenzamide and aromatic aldehydes for the synthesis of 2,3-dihydroquinazolin-4(1*H*)-one, which is an important class of heterocyclic compounds (see Supporting Information Figure S29).[46] The Lewis acid and Brønsted acid sites can facilitate the deacetalization and acetalization reactions, respectively (Figure 4b).[47] The introduction of the OTf group drives the deacetalization of benzaldehyde dimethyl acetal to benzaldehyde in the presence of HP-UiO-66-NH_2-OTf or UiO-66-NH_2-OTf, while negligible conversion can be observed with UiO-66-NH_2 nor HP-UiO-66-NH_2 (Figure 4c). Owing to the acid sites involved in the hierarchically porous structure, enhanced mass transfer and reaction performance would be expected from HP-UiO-66-NH_2-OTf (see Supporting Information Figure S26). The microporous MOF, UiO-66-NH_2-OTf, gives 30% conversion and 40% selectivity only as the restricted micropores are unfavorable to the mass transfer and conversion (Figure 4c). In contrast, 99% conversion with 81% selectivity to the target product can be achieved over HP-UiO-66-NH_2-OTf. The high conversion and selectivity are maintained in the three catalytic cycles, and the MOF crystallinity is well retained after the reaction, as demonstrated by the powder X-ray diffraction (PXRD) pattern (Figure 4d and see Supporting Information Figure S30). All of the above results highlight that the integrated advantages of the ordered micropores and the defective mesopores as well as the strong acidity in HP-UiO-66-NH_2-OTf are responsible for the excellent performance in tandem catalysis.

Conclusion

In summary, a simple yet efficient rigid modulator-assisted strategy is developed to convert the microporous MOFs into their corresponding HP-MOFs with mesoporous structures and well-retained stability. The resulting HP-MOFs possess uncoordinated carboxyl groups dangling on the skeleton. By subsequently modifying the OTf unit onto the Zr-oxo clusters, the one-pot cascade reactions can be promoted by taking advantage of the acid sites and hierarchical pores in HP-UiO-66-NH_2-OTf. This versatile synthetic strategy opens a new avenue to the creation of MP-MOFs with undisturbed stability and pushes them one step forward toward enhanced applications.

Supporting Information

Supporting Information is available and includes detailed experimental procedures and additional figures.

Conflict of Interest

There is no conflict of interest to report.

Acknowledgments

This work was supported by The National Key Research and Development Program of China (grant no. 2021YFA1500400), the NSFC (grant nos. 21725101, 22161142001, and 22001242), and the Fundamental Research Funds for the Central Universities (grant nos. WK3450000007 and WK2060000038).

References

1. Furukawa, H.; Cordova, K. E.; O'Keeffe, M.; Yaghi, O. M. The Chemistry and Applications of Metal–Organic Frameworks. *Science* **2013**, *341*, 1230444.
2. Jiao, L.; Seow, J. Y. R.; Skinner, W. S.; Wang, Z. U.; Jiang H.-L. Metal–Organic Frameworks: Structures and Functional Applications. *Mater. Today* **2019**, *27*, 43–68.
3. Li, B.; Wen, H.-M.; Cui, Y.; Zhou, W.; Qian, G.; Chen, B. Emerging Multifunctional Metal–Organic Framework Materials. *Adv. Mater.* **2016**, *28*, 8819–8860.
4. Zhou, H.-C.; Kitagawa, S. Metal–Organic Frameworks (MOFs). *Chem. Soc. Rev.* **2014**, *43*, 5415.
5. Zhao, X.; Wang, Y.; Li, D.-S.; Bu, X.; Feng, P. Metal–Organic Frameworks for Separation. *Adv. Mater.* **2018**, *30*, 1705189.

DOI: 10.31635/ccschem.022.202201974
Citation: *CCS Chem.* **2022**, 4, 3705–3714
Link to VoR: https://doi.org/10.31635/ccschem.022.202201974

6. Jiao, L.; Wang, J.; Jiang, H.-L. Microenvironment Modulation in Metal–Organic Framework-Based Catalysis. *Acc. Mater. Res.* **2021**, *2*, 327.
7. Li, L.; Lin, R.-B.; Krishna, R.; Xiang, S.; Wu, H.; Li, J.; Zhou, W.; Chen, B. Ethane/Ethylene Separation in a Metal–Organic Framework with Iron-Peroxo Sites. *Science* **2018**, *362*, 443–446.
8. Wang, H.; Li, J. Microporous Metal–Organic Frameworks for Adsorptive Separation of C5-C6 Alkane Isomers. *Acc. Chem. Res.* **2019**, *52*, 1968–1978.
9. Cong, S.; Yuan, Y.; Wang, J.; Wang, Z.; Kapteijn, F.; Liu, X. Highly Water-Permeable Metal–Organic Framework MOF-303 Membranes for Desalination. *J. Am. Chem. Soc.* **2021**, *143*, 20055–20058.
10. Li, P.; Modica, J. A.; Howarth, A. J.; Vargas, L. E.; Moghadam, P. Z.; Snurr, R. Q.; Mrksich, M.; Hupp, J. T.; Farha, O. K. Toward Design Rules for Enzyme Immobilization in Hierarchical Mesoporous Metal–Organic Frameworks. *Chem* **2016**, *1*, 154–169.
11. Sun, J.; Zhang, X.; Zhang, D.; Chen, Y.-P.; Wang, F.; Li, L.; Liu, T.-F.; Yang, H.; Song, J.; Cao, R. Building Block Symmetry Relegation Induces Mesopore and Abundant Open-Metal Sites in Metal–Organic Frameworks for Cancer Therapy. *CCS Chem.* **2021**, *3*, 1048–1058.
12. Teng, J.; Chen, M.; Xie, Y.; Wang, D.; Jiang, J.-J.; Li, G.; Wang, H.-P.; Fan, Y.; Wei, Z.-W.; Su, C.-Y. Hierarchically Porous Single Nanocrystals of Bimetallic Metal-Organic Framework for Nanoreactors with Enhanced Conversion. *Chem. Mater.* **2018**, *30*, 6458–6468.
13. Zhang, P.; Chen, C.; Kang, X.; Zhang, L.; Wu, C.; Zhang, J.; Han, B. In Situ Synthesis of Sub-Nanometer Metal Particles on Hierarchically Porous Metal–Organic Frameworks via Interfacial Control for Highly Efficient Catalysis. *Chem. Sci.* **2018**, *9*, 1339–1343.
14. Yue, Y.; Fulvio, P. F.; Dai, S. Hierarchical Metal–Organic Framework Hybrids: Perturbation-Assisted Nanofusion Synthesis. *Acc. Chem. Res.* **2015**, *48*, 3044–3052.
15. Deng, H.; Grunder, S.; Cordova, K. E.; Valente, C.; Furukawa, H.; Hmadeh, M.; Gandara, F.; Whalley, A. C.; Liu, Z.; Asahina, S.; Kazumori, H.; O'Keeffe, M.; Terasaki, O.; Stoddart, J. F.; Yaghi, O. M. Large-Pore Apertures in a Series of Metal–Organic Frameworks. *Science* **2012**, *336*, 1018–1023.
16. Li, T.; Kozlowski, M. T.; Doud, E. A.; Blakely, M. N.; Rosi, N. L. Stepwise Ligand Exchange for the Preparation of a Family of Mesoporous MOFs. *J. Am. Chem. Soc.* **2013**, *135*, 11688–11691.
17. Chen, Z.; Li, P.; Wang, X.; Otake, K. I.; Zhang, X.; Robison, L.; Atilgan, A.; Islamoglu, T.; Hall, M. G.; Peterson, G. W.; Stoddart, J. F.; Farha, O. K. Ligand-Directed Reticular Synthesis of Catalytically Active Missing Zirconium-Based Metal–Organic Frameworks. *J. Am. Chem. Soc.* **2019**, *141*, 12229–12235.
18. Pang, J.; Di, Z.; Qin, J.-S.; Yuan, S.; Lollar, C. T.; Li, J.; Zhang, P.; Wu, M.; Yuan, D.; Hong, M.; Zhou, H.-C. Precisely Embedding Active Sites into a Mesoporous Zr-Framework through Linker Installation for High-Efficiency Photocatalysis. *J. Am. Chem. Soc.* **2020**, *142*, 15020–15026.
19. Yang, L.; Cai, P.; Zhang, L.; Xu, X.; Yakovenko, A. A.; Wang, Q.; Pang, J.; Yuan, S.; Zou, X.; Huang, N.; Huang, Z.; Zhou, H.-C. Ligand-Directed Conformational Control over Porphyrinic Zirconium Metal–Organic Frameworks for Size-Selective Catalysis. *J. Am. Chem. Soc.* **2021**, *143*, 12129–12137.
20. Ding, M.; Cai, X.; Jiang, H.-L. Improving MOF Stability: Approaches and Applications. *Chem. Sci.* **2019**, *10*, 10209–10230.
21. Jiang, H.-L.; Makal, T. A.; Zhou, H.-C. Interpenetration Control in Metal–Organic Frameworks for Functional Applications. *Coord. Chem. Rev.* **2013**, *257*, 2232–2249.
22. Ferguson, A.; Liu, L.; Tapperwijn, S. J.; Perl, D.; Coudert, F.-X.; Cleuvenbergen, S. V.; Verbiest, T.; van der Veen, M. A.; Telfer, S. G. Controlled Partial Interpenetration in Metal–Organic Frameworks. *Nat. Chem.* **2016**, *8*, 250–257.
23. Feng, L.; Yuan, S.; Qin, J.-S.; Wang, Y.; Kirchon, A.; Qiu, D.; Cheng, L.; Madrahimov, S. T.; Zhou, H.-C. Lattice Expansion and Contraction in Metal–Organic Frameworks by Sequential Linker Reinstallation. *Matter* **2019**, *1*, 156–167.
24. Feng, L.; Wang, K.-Y.; Lv, X.-L.; Yan, T.-H.; Zhou, H.-C. Hierarchically Porous Metal–Organic Frameworks: Synthetic Strategies and Applications. *Natl. Sci. Rev.* **2020**, *7*, 1743–1758.
25. Bradshaw, D.; El-Hankari, S.; Lupica-Spagnolo, L. Supramolecular Templating of Hierarchically Porous Metal–Organic Frameworks. *Chem. Soc. Rev.* **2014**, *43*, 5431–5443.
26. Yan, R.; Zhao, Y.; Yang, H.; Kang, X.-J.; Wang, C.; Wen, L.-L.; Lu, Z.-D. Ultrasmall Au Nanoparticles Embedded in 2D Mixed-Ligand Metal–Organic Framework Nanosheets Exhibiting Highly Efficient and Size-Selective Catalysis. *Adv. Funct. Mater.* **2018**, *28*, 1802021.
27. Cai, G.; Yan, P.; Zhang, L.; Zhou, H.-C.; Jiang, H.-L. Metal–Organic Framework-Based Hierarchically Porous Materials: Synthesis and Applications. *Chem. Rev.* **2021**, *121*, 12278–12326.
28. Wang, K.-Y.; Feng, L.; Yan, T.-H.; Wu, S.; Joseph, E. A.; Zhou, H.-C. Rapid Generation of Hierarchically Porous Metal–Organic Frameworks through Laser Photolysis. *Angew. Chem. Int. Ed.* **2020**, *59*, 11349–11354.
29. Meng, F.; Zhang, S.; Ma, L.; Zhang, W.; Li, M.; Wu, T.; Li, H.; Zhang, T.; Lu, X.; Huo, F.; Lu, J. Construction of Hierarchically Porous Nanoparticles@Metal–Organic Frameworks Composites by Inherent Defects for the Enhancement of Catalytic Efficiency. *Adv. Mater.* **2018**, *30*, 1803263.
30. Li, K.; Lin, S.; Li, Y.; Zhuang, Q.; Gu, J. Aqueous-Phase Synthesis of Mesoporous Zr-Based MOFs Templated by Amphoteric Surfactants. *Angew. Chem. Int. Ed.* **2018**, *57*, 3439–3443.
31. Yuan, S.; Zou, L.; Qin, J. S.; Li, J.; Huang, L.; Feng, L.; Wang, X.; Bosch, M.; Alsalme, A.; Cagin, T.; Zhou, H.-C. Construction of Hierarchically Porous Metal–Organic Frameworks through Linker Labilization. *Nat. Commun.* **2017**, *8*, 15356.
32. McNamara, N. D.; Hicks, J. C. Chelating Agent-Free; Vapor-Assisted Crystallization Method to Synthesize Hierarchical Microporous/Mesoporous MIL-125 (Ti). *ACS Appl. Mater. Interfaces* **2015**, *7*, 5338–5346.
33. Feng, L.; Yuan, S.; Zhang, L.-L.; Tan, K.; Li, J.-L.; Kirchon, A.; Liu, L.-M.; Zhang, P.; Han, Y.; Chabal, Y. J.; Zhou, H.-C.

DOI: 10.31635/ccschem.022.202201974
Citation: *CCS Chem.* **2022**, 4, 3705–3714
Link to VoR: https://doi.org/10.31635/ccschem.022.202201974

Creating Hierarchical Pores by Controlled Linker Thermolysis in Multivariate Metal–Organic Frameworks. *J. Am. Chem. Soc.* **2018**, *140*, 2363–2372.
34. Shen, K.; Zhang, L.; Chen, X.; Liu, L.; Zhang, D.; Han, Y.; Chen, J.; Long, J.; Luque, R.; Li, Y.; Chen, B. Ordered Macro-Microporous Metal–Organic Framework Single Crystals. *Science* **2018**, *359*, 206–210.
35. Cai, G.; Jiang, H.-L. A Modulator-Induced Defect-Formation Strategy to Hierarchically Porous Metal–Organic Frameworks with High Stability. *Angew. Chem. Int. Ed.* **2017**, *56*, 563–567.
36. Cai, G.; Ma, X.; Kassymova, M.; Sun, K.; Ding, M.; Jiang, H.-L. Large-Scale Production of Hierarchically Porous Metal–Organic Frameworks by a Reflux-Assisted Post-Synthetic Ligand Substitution Strategy. *ACS Cent. Sci.* **2021**, *7*, 1434–1440.
37. Hao, L.; Li, X.; Hurlock, M. J.; Tu, X.; Zhang, Q. Hierarchically Porous UiO-66: Facile Synthesis, Characterization and Application. *Chem. Commun.* **2018**, *54*, 11817–11820.
38. Taddei, M.; Wakeham, R. J.; Koutsianos, A.; Andreoli, E.; Barron, A. R. Post-Synthetic Ligand Exchange in Zirconium-Based Metal-Organic Frameworks: Beware of The Defects! *Angew. Chem. Int. Ed.* **2018**, *57*, 11706–11710.
39. Shen, T.; Gao, M.; Zang, W.; Ding, F.; Wang, J. Architecting Organo Silica Nanosheets for Regenerable Cost-Effective Organics Adsorbents. *Chem. Eng. J.* **2018**, *331*, 211–220.
40. Zhao, X.; Liu, S.; Tang, Z.; Niu, H.; Cai, Y.; Meng, W.; Wu, F.; Giesy, J. P. Synthesis of Magnetic Metal–Organic Framework (MOF) for Efficient Removal of Organic Dyes from Water. *Sci. Rep.* **2015**, *5*, 11849.
41. Prochowicz, D.; Nawrocki, J.; Terlecki, M.; Marynowski, W.; Lewinski, J. Facile Mechanosynthesis of the Archetypal Zn-Based Metal–Organic Frameworks. *Inorg. Chem.* **2018**, *57*, 13437–13442.
42. Hu, X.-J.; Li, Z.-X.; Xue, H.; Huang, X.; Cao, R.; Liu, T.-F. Designing a Bifunctional Brønsted Acid-Base Heterogeneous Catalyst through Precise Installation of Ligands on Metal–Organic Frameworks. *CCS Chem.* **2019**, *1*, 616–622.
43. Feng, X.; Jena, H. S.; Krishnaraj, C.; Arenas-Esteban, D.; Leus, K.; Wang, G.; Sun, J.; Ruscher, M.; Timoshenko, J.; Roldan Cuenya, B.; Bals, S.; Voort, P. V. Creation of Exclusive Artificial Cluster Defects by Selective Metal Removal in the (Zn, Zr) Mixed-Metal UiO-66. *J. Am. Chem. Soc.* **2021**, *143*, 21511–21518.
44. Zhang A. A.; Cheng X.; He X.; Liu W.; Deng S.; Cao R.; Liu T.-F. Harnessing Electrostatic Interactions for Enhanced Conductivity in Metal–Organic Frameworks. *Research* **2021**, *2021*, 9874273.
45. Vermoortele, F.; Vandichel, M.; Van de Voorde, B.; Ameloot, R.; Waroquier, M.; Van Speybroeck, V.; De Vos, D. E. Electronic Effects of Linker Substitution on Lewis Acid Catalysis with Metal–Organic Frameworks. *Angew. Chem. Int. Ed.* **2012**, *20*, 4887–4890.
46. Rueping, M.; Antonchick, A. P.; Sugiono, E.; Grenader, K. Asymmetric Brønsted Acid Catalysis: Catalytic Enantioselective Synthesis of Highly Biologically Active Dihydroquinazolinones. *Angew. Chem. Int. Ed.* **2009**, *48*, 908–910.
47. Gong, W.; Chen, X.; Jiang, H.; Chu, D.; Cui, Y.; Liu, Y. Highly Stable Zr(IV)-Based Metal–Organic Frameworks with Chiral Phosphoric Acids for Catalytic Asymmetric Tandem Reactions. *J. Am. Chem. Soc.* **2019**, *141*, 7498–7508.

DOI: 10.31635/ccschem.022.202201974
Citation: *CCS Chem.* **2022**, 4, 3705–3714
Link to VoR: https://doi.org/10.31635/ccschem.022.202201974